



Québec, QC
10 au 13 juin 2008 / June 10-13, 2008

Exploratory Study of Seismic Behaviour of Repaired Beam-Column Joints Reinforced with Superelastic Shape Memory Alloys

M. Shahria Alam, Moncef Nehdi and Maged A. Youssef
Department of Civil and Environmental Engineering, The University of Western Ontario,
London, Ontario, Canada, N6A 5B9

Résumé / Abstract : The objective of this study is to evaluate the seismic performance of a repaired concrete Beam-Column Joint (BCJ) specimen reinforced with superelastic (SE) Shape Memory Alloy (SMA) rebar. A large-scale BCJ reinforced with SMA rebars in the plastic-hinge zone was tested under reversed cyclic loading. Then the joint was repaired and retested. The joint was selected from an eight-storey RC building located in the high seismic region of western Canada and designed and detailed according to the NBCC 2005 and CSA A23.3-04 recommendations. The behaviour of the original and repaired joints under reversed cyclic loading, their load-storey drift, and energy dissipation ability were compared. The results demonstrate that SMA-RC BCJs are able to recover nearly all of their post-yield deformation requiring minimum amount of repairing even after a large earthquake.

1. Introduction

In many cases, strong earthquakes have caused severe damages to RC beam-column joints (BCJs) in the past. These BCJs are still considered extremely vulnerable during such earthquake events (Saatcioglu et al. 1999). In conventional seismic design of RC structures, reinforcing bars are expected to yield to dissipate the seismic energy, which result in permanent deformations. Earthquake resistant structures need to be sufficiently ductile as it is difficult and costly to build structures that can perform elastically under strong ground motion. Superelastic Shape Memory Alloys (SE SMAs) are unique alloys with the ability to undergo large deformations and return to their undeformed shape by removal of stresses. Therefore, SE SMAs have a great potential to be used as reinforcing bars. When used as reinforcement in critical structural elements along with conventional steel, SMA can undergo large inelastic strains caused by seismic loads, but potentially recover deformations at the end of the earthquake (Saiidi and Wang 2006). Their high strength, large energy hysteretic behaviour, full recovery of strains up to about 8%, and high resistance to corrosion and fatigue make them strong contenders for use in earthquake resistant structures (Wilson and Wesolowsky 2005). In particular, Ni-Ti alloy has been found to be the most promising SMA for seismic applications.

Because of its higher cost, it was not until 2004 that SMA found its way as reinforcement in RC structures. Saiidi and Wang (2006) designed two ¼-scale spiral RC columns with SMA longitudinal reinforcement in the plastic hinge area for laboratory shake table testing. Each specimen was subjected to a series of scaled motion amplitudes. The SMA RC columns were found superior to the conventional steel RC columns in limiting relative column top displacement and residual displacements. Also they withstood larger earthquake amplitudes than that of the conventional ones. The shake table data showed that SMA RC columns were able to recover nearly all of the post-yield deformation, thus requiring minimal repair.

Alam et al. (2007) demonstrated the potential of developing smart RC bridges utilizing SMAs as reinforcement and/or prestressing tendons.

This paper reports the seismic behaviour of an RC beam-column joint reinforced with SE SMAs in conjunction with steel where SMAs are specifically placed in the plastic hinge zone of the beam. The BCJ specimen was designed and constructed according to current seismic design standards, and tested under reversed cyclic loading. Then the joint was repaired with structural repair concrete and retested under similar loading. Therefore, the objectives of this study include the investigation of the performance of the repaired SE SMA RC BCJ under reversed cyclic loading and compare its performance to that of the original one.

2. Failure Mechanism of Beam-Column Joints

A number of researchers e.g. Hanson and Connor (1967), Megget and Park (1971), Meinheit and Jirsa (1981), Meggeta (2003) and others devoted significant effort studying the behaviour of joints, as well as on the development of design recommendations for ensuring adequate connection behaviour in frame structures expected to undergo large inelastic deformations. BCJ deficiencies may be categorized into three ways. First, weak column/strong beam, which contradicts failure hierarchy of the design capacity concept; when plastic hinges form in the columns, the axial force causes a rapid degradation of the ability of the hinge to absorb energy, while undergoing cyclic motion. Second, a weak beam/strong column – most favourable case since it is not associated with the loss of axial load carrying capacity, i.e. failure in the beam is less critical than that in the column. Finally, hinging in the joint, being at the point of intersection of the beam and column allows excessive rotations both in the beam and column in conjunction with a loss of load carrying capacity of the column. Such a hazardous failure mechanism is unacceptable and must be prevented in design. Therefore, beam-column joints require special attention for proper design and detailing works.

3. New Design Philosophy for Beam-Column Joints

Conventional structures are mostly designed for safety conditions, where earthquake energies are dissipated through yielding of reinforcement and its inelastic deformation. Structures are allowed to undergo severe damage, which means saving lives at the expense of structures incurring huge economic losses. More recently the vision has been broadened where the designers no longer want to surrender their own creations/constructions. The seismic design of structures has evolved towards performance-based design in which there is a need for new structural members and systems that possess enhanced deformation capacity and ductility, higher damage tolerance, concrete confinement, decreased or minimized residual crack sizes, recovered and reduced permanent deformations. If SE SMA is used as reinforcement instead of steel in the desired hinge locations of beams, it will not only be able to dissipate adequate seismic energy, but will also restore its original shape after a seismic event.

4. Experimental Program

Two large-scale BCJ specimens were constructed and tested at the Structures Laboratory of the University of Western Ontario. The specimens (JBC-2 and JBC-3) were reinforced with SE SMA at the plastic hinge region of the beam along with regular steel in the remaining portion of the joint. An eight-storey RC building with moment resisting frames was considered in this study, which was assumed to be located in the western part of Canada on firm ground with un-drained shear strength of more than 100 kPa. The elevation and plan of the building are shown in Fig. 1. It was designed and detailed in accordance with Canadian Standards (2004). The design Peak Ground Acceleration (PGA) was 0.54g and the moment frames were designed with a moderate level of ductility. An exterior BCJ was isolated at the points of contra-flexure, from mid-height of fifth floor to mid-height of sixth floor (Joint A in Fig. 1). The size of the BCJ test specimen was reduced by a factor of $\frac{3}{4}$ to account for the laboratory space and

limitations of testing equipments. The forces acting on the joint were also scaled down by a factor of $(\frac{3}{4})^2$. This factor was chosen to maintain stresses in the scaled models similar to that of the full-scale joint.

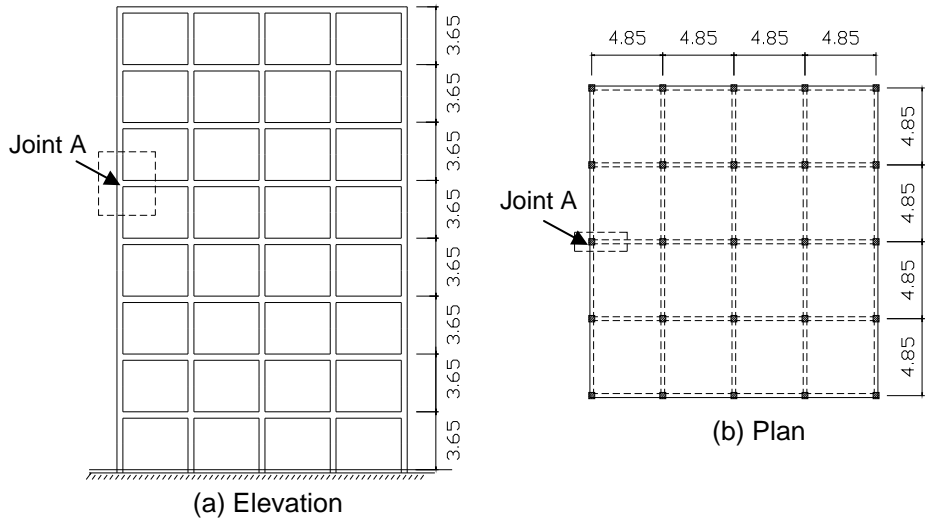


Figure 1 - Eight-storey frame building located in the western part of Canada (dimensions in meters).

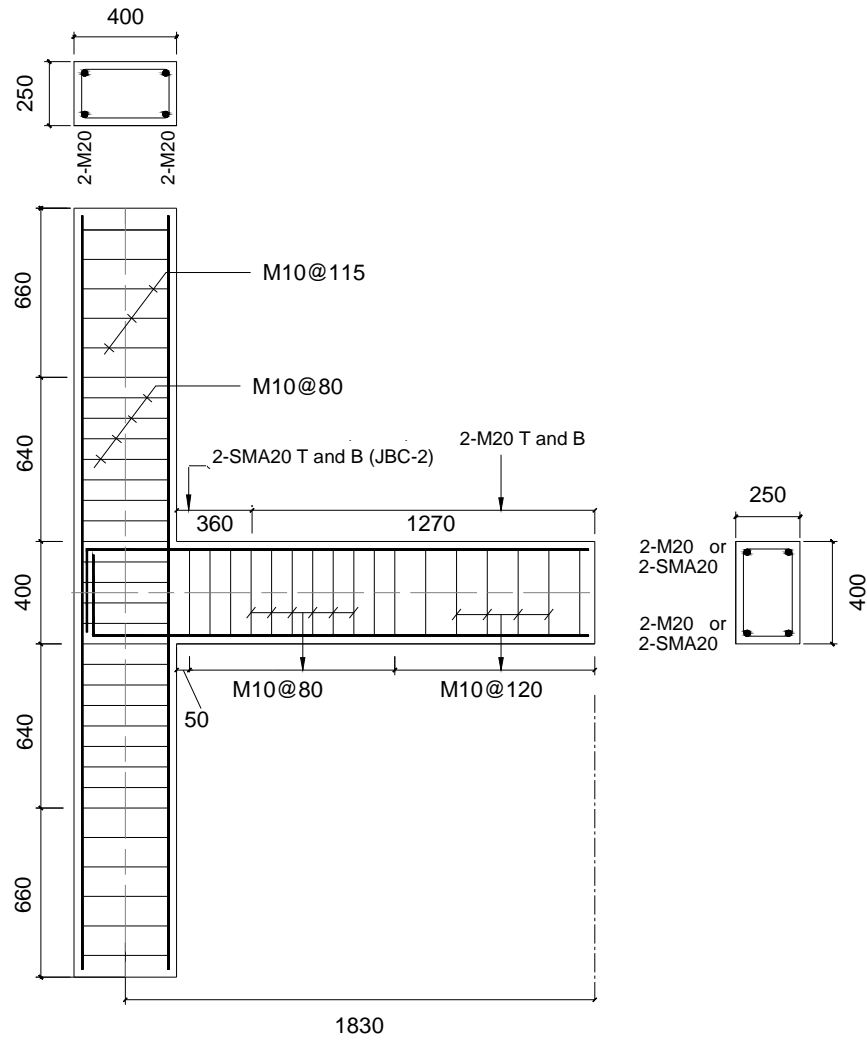


Figure 2 - Reinforcement details of specimens JBC-2 and JBC-3 (all dimensions in mm).

4.1 Details of the Specimens

First the frame was analyzed considering all possible load combinations. Based on the analysis results, the beam and column were designed for maximum moments and shear forces. The design column axial force, P , was 620 kN leading to a scaled down P of 350 kN. The detailed design of joint JBC-2 and JBC-3 are given in Fig. 2. Specimen JBC-2 was constructed in conventional way. The only difference was in the use of SE SMA longitudinal reinforcement at the plastic hinge region instead of regular steel. The top and bottom longitudinal reinforcement for the beam are 2-M20 rebars and 2-SE SMA20 (20.6 mm in diameter) rebars at different section as shown in Fig. 2. The plastic hinge length was calculated as 360 mm^{12} from the face of the column. Mechanical couplers were used to connect SMA rebars and regular steel rebars. The total length of SMA rebars was 450 mm (centre to centre of the couplers). The size of the longitudinal rebar and the size and spacing of the transverse reinforcement for the joint conform to current code requirements (CSA 2004).

The specimen was cast with highly flowable ready-mix concrete. The concrete compressive strength at the time of testing was 53.7 MPa. The split cylinder tensile strength was 2.8 MPa. Tensile strength tests of steel rebars were also performed in the laboratory. The yield strength, ultimate strength, and Young's modulus were 450 MP, 650 MPa, and 193 GPa. The steel rebars used for ties were 20M and 10M with a yield strength and ultimate strength of 422 MPa and 682 MPa, respectively.

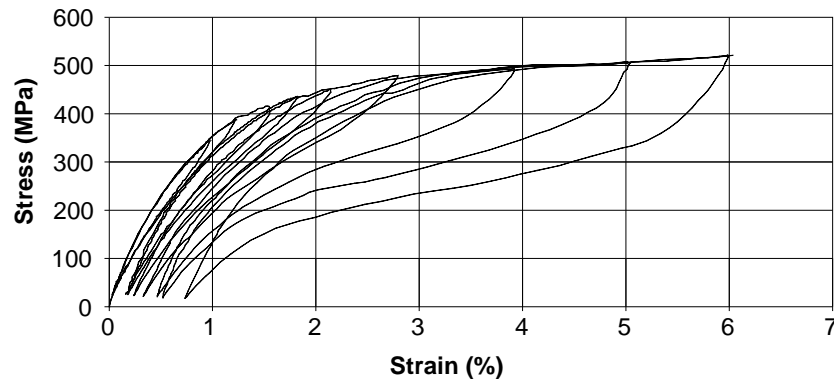


Figure 3 - Cyclic tensile strength of SE SMA rebar within couplers.

Equiatomic Ni-Ti alloy rebar was used as reinforcement in the plastic hinge region of the beam. Its austenite finish temperature, A_f , defining the complete transformation from martensite to austenite, ranges from -15°C to -10°C . Each Ni-Ti bar used in this study was 450 mm long and 20.6 mm in diameter. Each end of the rebar was inserted into the coupler over a length of 45 mm. Figure 3 shows the experimental cyclic tensile behaviour of a Ni-Ti bar within couplers at room temperature. The characteristic stress-strain curve shows a flag-shaped response. Its Young's modulus (E) is calculated as 62.5 GPa. The rebar was tested up to a maximum of 6% strain and a residual strain of 0.73% was observed.

4.2 Test Setup and Instrumentation

Figure 4 illustrates the schematic diagram of the specimen, the test rig, and the reaction frame. The bottom of the column was hinged with pins penetrating through a sleeve with narrow holes. A roller support was created at the top of the column with pins penetrating through a sleeve with 20 mm vertical slots. The load cycles were applied at the beam tip using an actuator, which was pin connected at the beam-tip. The arm length was measured as 1870 mm from the pin connection to the mid column line. Figure 4 also illustrates the instrumentation of test specimens. Two load cells were used to measure the column axial load and beam tip load. During testing, displacements were measured at various locations using linear variable displacement transducers (LVDTs). One pair of LVDT was attached to the joint area to measure the joint distortion. The other two LVDTs were placed in parallel on top and bottom of the beam at a distance of 180 mm away from the column face to measure beam rotation. The displacement

was measured at the free end of the beam using a string potentiometer. A portable computer attached to the data acquisition system was used to record readings at a constant time interval with one reading per second.

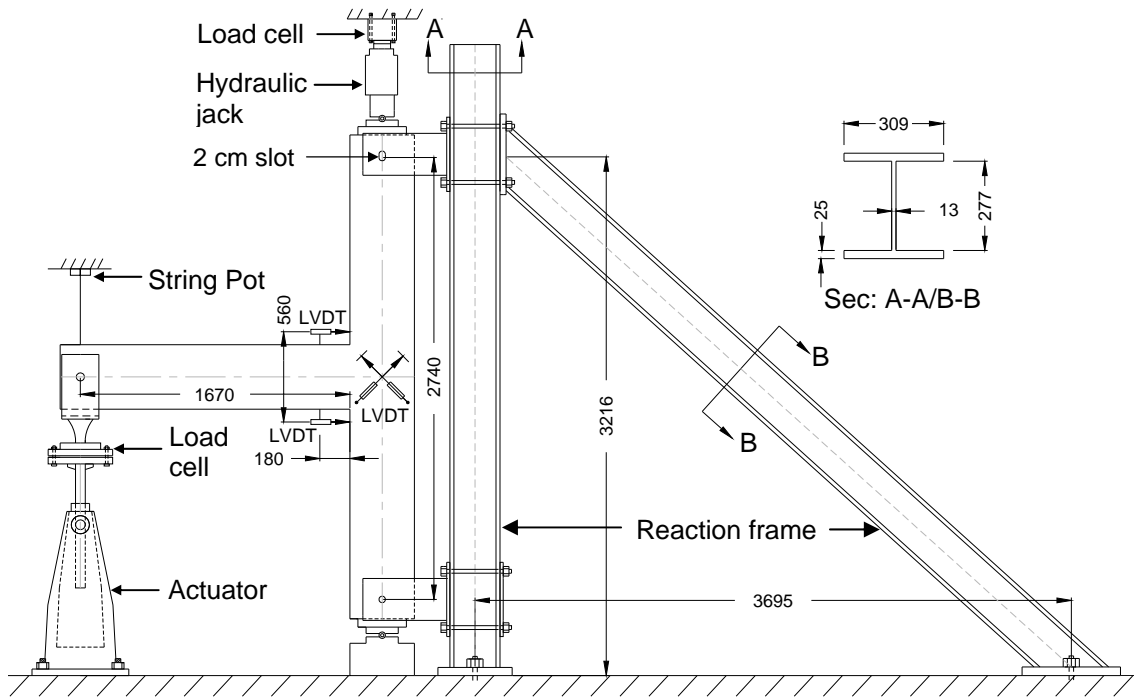


Figure 4 - Test setup.

Figure 4 illustrates the schematic diagram of the specimen, the test rig, and the reaction frame. The bottom of the column was hinged with pins penetrating through a sleeve with narrow holes. A roller support was created at the top of the column with pins penetrating through a sleeve with 20 mm vertical slots. The load cycles were applied at the beam tip using an actuator, which was pin connected at the beam-tip. The arm length was measured as 1870 mm from the pin connection to the mid column line. Figure 4 also illustrates the instrumentation of test specimens. Two load cells were used to measure the column axial load and beam tip load. During testing, displacements were measured at various locations using linear variable displacement transducers (LVDTs). One pair of LVDT was attached to the joint area to measure the joint distortion. The other two LVDTs were placed in parallel on top and bottom of the beam at a distance of 180 mm away from the column face to measure beam rotation. The displacement was measured at the free end of the beam using a string potentiometer. A portable computer attached to the data acquisition system was used to record readings at a constant time interval with one reading per second.

4.3 Loading

While testing the BCJ, constant axial load was applied at the top of the column and reversed quasi-static cyclic load was applied at the beam tip. The load history applied at the beam tip was divided into two phases where a load-controlled phase was followed by a displacement-controlled loading phase. During the load-controlled phase, two load cycles were applied at 10% of the theoretical yield load of the beam to ensure that the data acquisition system is functioning properly. The following load control cycles (4 cycles) were applied to define the loads causing flexural cracking in the beam (2 cycles) and yielding of its longitudinal rebars (2 cycles). The yield load, P_y , and the yield displacement, Δ_y , were recorded. After yielding, displacement-controlled loading was applied in the form of incremental multiplies of the yield

displacement, Δ_y . In order to verify a stable condition, for each load cycle the test specimen was subjected to two complete cycles. Tests were conducted up to a storey drift of 7.9%, which is more than double the collapse limit (Elnashai and Broderick (1994)).

5. Test Results

This section describes the behaviour of specimens JBC-2 and JBC-3 under reversed cyclic loading.

5.1 Behaviour of JBC-2

Figure 5 shows the load-storey drift relationship of the SMA-RC beam-column joint specimen JBC-2. At a drift of 0.22%, the bottom of the beam at 160 mm away from the column face experienced the First Flexural Crack (FFC). As the loading progressed several flexural cracks occurred at the top and bottom of the beam along a length of 1300 mm measured from the column face. At a drift of 0.66% and a beam tip-load of 18 kN, a small crack appeared at the bottom edge of the joint region near the column face. A fine crack took place along the diagonal of the joint at a beam tip-load of 22 kN corresponding to a drift of 1.12%. It was observed that the bottom SMA rebar reached its yield strain at a beam tip-load of 32.7 kN and a drift of 1.97%. In this case, the corresponding yield displacement, Δ_y was observed as 18 mm. At a deformation level of $2\Delta_y$, the existing flexural cracks started to propagate further deeper into the beam. At a deformation level of $3\Delta_y$, the FFC opened up to 7.4 mm and later closed to a width of less than 1 mm. Several existing flexural cracks in the beam extended to its full depth parallel to the column face. At a deformation level of $4\Delta_y$, the cracks became wider in the plastic hinge area of the beam. The FFC opened up to 10.7 mm during the loading cycle, and part of the bottom concrete cover spalled off. At the end of this cycle, the residual FFC crack width was 2.2 mm, whereas all other cracks in the beam had very small width. The joint region was having few diagonal cracks of very fine width and small length and remained almost fully intact.

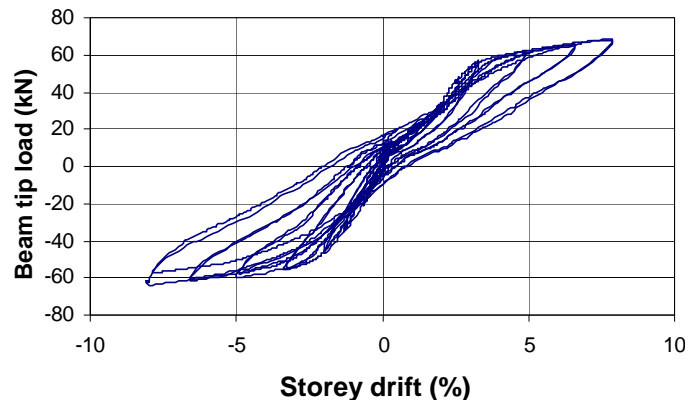


Figure 5 - Beam tip load-storey drift relationship of specimens JBC-2.

5.2 Repairing of JBC-2 and Testing of JBC-3

Besides some minor cracks in the beam of JBC-2, there was one major crack at half beam depth away from the column face with substantial loss of cover concrete on its top and bottom face. The repairing technique includes the removal of damaged concrete, placing concrete grout in the removed zone, and injecting epoxy in all accessible minor cracks. After curing the concrete for 7 days, the repaired specimen JBC-3 was mounted on the test rig and subjected to reversed cyclic loading.

5.3 Behaviour of JBC-3

The behaviour of specimen JBC-3 was found similar to that of JBC-2. Figure 6 shows its beam tip load versus storey drift relationship. The first flexural crack (FFC) was observed at the top of the beam at a distance of 250 mm (9.84 in) away from the column face at a beam tip-load of 14.5 kN (3.26 kip) corresponding to a drift of 0.52%. The FFC did not occur at the cold joint region, but rather took place at the middle of the repaired section. This indicates the excellent bonding between the old and new concrete. Additional cracks occurred along the beam length with the progress of loading. The joint region was almost fully intact with very few cracks of fine width. The top longitudinal rebar of the beam first yielded at a beam tip-load of 42.7 kN (9.61 kip) with a corresponding yield displacement, Δ_y of 18 mm (0.71 in, drift of 1.97%). As the loading increased, the FFC started to grow wider. At 3.3% drift, the FFC became 6 mm (0.24 in) wide at the top, while in the reversed direction at the same drift, the crack size was 4 mm (0.16 in) at the bottom. At a displacement of $3.3\Delta_y$ (6.6% drift), the specimen suffered a 10 mm (0.39 in) wide crack at the top, and a 9 mm (0.35 in) crack at the bottom while in the reversed direction. At a drift of $4\Delta_y$ (7.9%), the FFC at the top became 19 mm (0.75 in) wide whereas the bottom experienced a 16 mm (0.63 in) wide crack. At this stage, some concrete cover from the top and bottom part of the beam started to spall off and the stirrups at the repaired section became visible. Throughout the test, the axial load of the column was maintained and the joint area remained fully undamaged apart from a few hairline cracks.

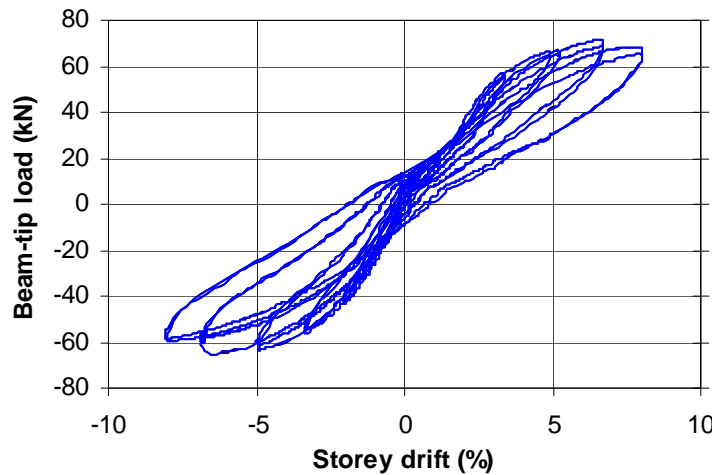


Fig. 6 – Beam-tip load-storey drift relationship of specimen JBC-3.

5.4 Performance between Original and Repaired Specimen

Both load-storey drift relationships show typical elasto-plastic behaviour where both maintained a stable post-yield load carrying capacity throughout the test. They started with comparable initial stiffness and followed a similar trend. In the case of JBC-2, the load continuously increased with the increase of the storey-drift without showing any reduction in load-carrying capacity. On the other hand, JBC-3 showed a gradual decline in load carrying capacity beyond a storey-drift of 6.5%. At a storey-drift of 7.9%, JBC-2 was found to absorb 16.7 kN.m (12.32 kip.ft) of energy, whereas JBC-2 dissipated 16.5 kN.m (12.18 kip.ft) of energy at the same storey-drift, which is only 1.2% smaller than that of JBC-2. Thus, it is evident that the repaired specimen JBC-3 could dissipate an almost equal amount of energy to that of the original specimen, JBC-2.

6. Conclusions

This study examines the seismic performance a BCJ reinforced with SE SMA rebars in its plastic hinge region. It has observed that the flag-shaped hysteretic stress-strain curve of SE SMA rebar produced a flag-shaped force-displacement hysteretic shape for JBC-2. This resulted in very small residual displacements in the SE SMA-RC beam-column joint JBC-2. After testing JBC-2 under reversed cyclic loading, it was repaired with structural repair concrete and retested. The repaired specimen JBC-3 showed similar behaviour to that of the original one in terms of load-storey drift and energy dissipation capacity. This extraordinary characteristic of SE SMA-RC beam-column joints could have a great benefit in high seismic areas, where such RC joints would remain functional even after a strong earthquake. Thus, SE SMA rebars possess great potential to replace or complement conventional steel rebars achieving considerable gains in seismic performance and safety.

7. Acknowledgements

The authors gratefully acknowledge the donation of SE SMA bars from ATI Wah Chang Inc, Albany, OR and the funding provided by the Natural Sciences and Engineering Research Council of Canada (NSERC).

8. References and Standards

- Alam, M.S., Youssef, M.A. and Nehdi, M. 2007. Utilizing shape memory alloys to enhance the performance and safety of civil infrastructure: a review, *Canadian Journal of Civil Engineering*, 34:1075-1086.
- Alam, M.S., Nehdi, M. and Youssef, M.A. 2007. Shape memory alloy based smart RC bridge: overview of state of the art, *Smart Structures and Systems, An International Journal*, in press.
- CSA A23.3-04, 2004, *Design of Concrete Structures* (Canadian Standards Association, Rexdale, Ontario, Canada).
- Elnashai, A.S. and Broderick, B.M. 1994. Seismic resistance of composite beam-columns in multi-storey structures. Part 1: Experimental studies, *Journal of Constructional Steel Research*, 30:201-229.
- Hanson, N.W. and Connor, H.W. 1967. Seismic resistance of reinforced concrete beam-column joints, *Journal of the Structural Division, ASCE*, 93:533-560.
- Megget, L.M. and Park, R. 1971. Reinforced concrete exterior beam-column joints under seismic loading, *New Zealand Engineering (Wellington)*, 26:341-353.
- Meggeta, L.M. 2003. The seismic design and performance of reinforced concrete beam-column knee joints in buildings, *Earthquake Spectra*, 19:863-895.
- Meinheit, D.F., and Jirsa, J.O. 1981. Shear strength of RC beam-column connections, *Journal of Structural Division, ASCE*, 107:2227-2244.
- National Building Code of Canada, 2005. National Research Council, Canada.
- Paulay, T., and Priestley, M. N. J. 1992. *Seismic Design of Reinforced Concrete and Masonry Buildings* (John Wiley & Sons, Inc., New York).
- Saatcioglu, M., Mitchell, D., Tinawi, R., Gardner, N.J., Gillies, A.G., Ghobarah A., Anderson, D.L. and Lau, D. 2001. The August 17, 1999, Kocaeli (Turkey) earthquake - damage to structures, *Canadian Journal of Civil Engineering*, 28:715-737.
- Saiidi, M.S. and Wang, H. 2006. Exploratory study of seismic response of concrete columns with shape memory alloys reinforcement, *ACI Structural Journal*, 103:435-442.
- Wilson, J.C. and Wesolowsky, M.J. 2005. Shape memory alloys for seismic response modification: a state-of-the-art review, *Earthquake Spectra*, 21:569-601.